

## Macroscopic parameters and line shapes of a gas laser

Guy Stephan and Manfred Trümper

*Laboratoire de Spectroscopie (Equipe de Recherche No. 748 associée au Centre National de la Recherche Scientifique),  
Université de Rennes, avenue du Général Leclerc, F-35042 Rennes, France*

(Received 8 March 1984)

The theory of line shapes in monomode weak-gain gas lasers which we have developed recently shows that asymmetries of Lamb dips are governed by opposite lens effects which arise from population and saturation inhomogeneities. The competition between these effects depends on the geometrical characteristics of the laser. It is our aim in this paper to illustrate experimentally this fact with the 3.39- $\mu\text{m}$  line of a He-Ne laser. To get a strongly diverging beam we have chosen a quasihemispheric resonator whose length (57 cm) almost equals the radius of curvature of the concave mirror ( $R=60$  cm). The amplifying tube is about 20 cm long and is placed on the side of either the plane or the concave mirror, thus allowing us to vary the saturation inhomogeneity. In the first case the inhomogeneity is stronger and causes the maximum of intensity to be on the low-frequency side of the line, while in the second case population and saturation inhomogeneities are of the same order. We have repeated the experiment with two tubes having different internal diameters (8 and 4 mm) in order to vary the population effects. In the case of the narrower tube one observes a gradual passage from a low- to a high-frequency type of asymmetry when the discharge current is increased. This observation is explained by an increase of the lens effect due to saturation which overcomes the one due to population. Applying our previously developed theoretical methods, we find the results in qualitative agreement with these experiments.

### I. INTRODUCTION

Since its discovery in 1964 the Lamb dip,<sup>1-3</sup> a prominent feature of line profiles in weak-gain monomode gas lasers, has been studied extensively. Many phenomena contribute to the formation of line shapes and their investigation is still going on. We wish to recall briefly some of the main steps in the history of these investigations.

Lamb's theory of the mean saturating field predicted a symmetric line shape. However, experimental studies by Szöke and Javan,<sup>2,4</sup> by Smith,<sup>5</sup> and by Cordover and Bonczyk<sup>6</sup> showed an asymmetry which was first attributed to collisions,<sup>2-7</sup> i.e., to a microscopic origin. The asymmetry was also observed in a two-mode laser by Fork and Pollack,<sup>8</sup> but it varied from author to author and was not even observed in some cases.<sup>9</sup> According to experiments by White,<sup>10</sup> the center of the Lamb dip is displaced when current or pressure are varied. Theories used in these studies are based on the model of a "homogeneous laser." The field is modeled by plane waves and the optical properties of the amplifying medium do not depend on coordinates.

However, several authors, such as Troitskii and Chebotaev,<sup>11</sup> Mazanko *et al.*,<sup>12</sup> and Wolff *et al.*<sup>13</sup> measured the transverse and longitudinal variation of the linear gain in gas lasers and found that at weak discharge currents it was parabolic with a maximum on the laser axis. At strong currents the gain was found to decrease towards the axis. This phenomenon is due to the inhomogeneity of the population caused by collisions of atoms with others and with the wall. The radial profile of the level  $1s_5$  of neon has been measured by Schlie and Verdeyen<sup>14</sup> who found that the distribution was a parabola which had the zero at the wall of the discharge tube. The inhomogeneity

of the population of excited atoms was linked to the discharge current by Bennett.<sup>15</sup>

Concurrent with this work, the distribution of the electromagnetic field in the laser was studied, for instance, by Fox and Li<sup>16</sup> and by Kogelnik.<sup>17</sup> The latter author developed a matrix method which allowed calculation of the beam parameters in a cavity containing lenses. Casperson and Yariv<sup>18</sup> extended this linear theory to the case of a laser cavity with two plane mirrors. The amplifying medium is represented by a complex index of refraction with quadratic transverse variation. The asymmetry of the line profile is explained by the variation of the volume of the mode.

The population inhomogeneity is a linear effect, but there is also a nonlinear inhomogeneity effect due to the saturation of atoms which is proportional to the intensity of the field. It was invoked to explain the mechanism of filamentation of light in high-gain lasers<sup>19,20</sup> as a process of self-trapping or self-focusing. Freed and Haus<sup>21</sup> discussed the origins of Lamb-dip asymmetries in CO: They pointed out that a competition can occur between focusing and defocusing effects due to these linear and nonlinear transverse inhomogeneities. Maeda and Shimoda<sup>22</sup> introduced in the laser equations a transverse distribution of the population inversion and considered also the transverse inhomogeneity of saturation. Their conclusion was that the "self-focusing effect and the geometry of the resonator are found to significantly influence the shape of the Lamb dip." The influence of a diaphragm in a laser was noted by Garside.<sup>23</sup> The lens effects due to saturation vary with frequency and give rise to variations of the diameter of the mode. Diffraction losses caused by a diaphragm are then frequency dependent and thus another cause of asymmetry.

Summing up the history of work on asymmetries of line shapes, one may say that at the end of the 1970s the basic macroscopic effects which shape spectral lines in gas lasers were known, but had not been dealt with in a systematic or quantitative manner. Nevertheless, the interest in predictions of line shapes exists. For instance, a secondary frequency standard may be based on a He-Ne laser which is stabilized on the 3.39- $\mu\text{m}$  absorption line of methane. Barger and Hall<sup>24</sup> as well as Kramer *et al.*<sup>25</sup> observed an asymmetry and a displacement of the maximum of that line.

In 1981 Stephan and Taleb<sup>26</sup> described a theory of Gaussian beams in gas lasers where the field parameters are numerically calculated under the assumption that a homogeneous medium fills the entire cavity and that diffraction effects can be neglected. The complex lens effect of the amplifying medium modifies the wave-front curvature and the diameter of the mode, and the asymmetry of the line depends on the variation of these two parameters. The measured line shape then depends on the method which is used in the measurement.<sup>27</sup> The Garside effect has been observed in a monomode laser by Le Floch *et al.*,<sup>28</sup> who also studied experimentally<sup>29</sup> the influence of the distance between the mirrors on the line shape. The role played by length and position of the amplifying tube has been investigated by Stephan<sup>30</sup> and by Cérez and Felder.<sup>31</sup> In this work the saturating fields have been represented by their mean values.

We have recently proposed a theory of a monomode laser<sup>32</sup> in which both the transverse inhomogeneities of the population and the transverse and longitudinal variations of the saturation are taken into account, as well as the influence of the Garside effect, the geometrical parameters of the resonator, and diffraction by a diaphragm on the field distribution. Our methods allow for the numerical calculation of the spatial distribution of all parameters characterizing the field. We have applied our results to the question of whether a cavity geometry exists such that on one of the mirrors the beam has the same complex curvature  $q$  as the beam in the same passive resonator or, as we say, a geometry which stabilizes the transverse parameters of the output beam. The answer to this question has led us to a particular geometrical configuration<sup>33</sup> which has been successfully tested by experiments. There is another special case in which we have verified our theoretical results. As the asymmetry of a line depends on the competition between the inhomogeneities of population and saturation, we have looked at the case where the lens effects due to these inhomogeneities are of the same order, but opposite to each other. In that case one finds a quasisymmetric line. By varying the discharge current, an asymmetry of the line shape in either sense can be created.<sup>34</sup> Experiments on asymmetrical Lamb dips in a xenon laser have been published simultaneously to our work by Asami *et al.*<sup>35</sup> Their analysis includes the spatial gain distribution of the laser medium, the homogeneous broadening of the spectral line, and the saturation and atomic collision effects but neither the geometric nor self-focusing effects.

The purpose of this paper is to give some additional experimental proof for the applicability of our general

theory.<sup>32</sup> It is to be understood that we are concerned here with macroscopic properties of the laser which act on line shapes. We do not consider any property such as those described by Bordé *et al.*<sup>36</sup> We are using a laser with strong transverse and longitudinal variations of the field distribution. This feature allows us to change the relative weight of the contributions of the two types of inhomogeneities by varying the position of the amplifying tube. This tube is short as compared to the length of the resonator. In addition, we have used two tubes of different diameters to show the dependence of the effect on the radial distribution of population.

To render this paper more explicit we recall in Sec. II the principal ideas and equations developed in previous work. Then, in Sec. III, we describe our numerical and experimental results. We give a qualitative comparison between the observed asymmetries and the line shapes calculated for different values of the gain. We also give the variations of the diameter of the mode in different cases, showing that, in agreement with a previous prediction<sup>29</sup> by Le Floch *et al.*, it varies along the laser axis. Furthermore, we numerically calculate the variation of the curvature of wave fronts and show that it agrees with the predictions obtained from the Gaussian beam model.

## II. RESONATOR WITH AN INHOMOGENEOUS AMPLIFYING MEDIUM

In this section we recall some of the main equations and approximations which we have introduced in our previous work<sup>32,33</sup> to which we must refer for details. We are considering the model of a gas laser which is based on spatial distributions of fields, losses, and population.

The conditions for the field inside the cavity are obtained from Maxwell's equations by means of the paraxial approximation. We are using scaled coordinates  $\rho = r/W_0$  and  $\xi = cz/\omega W_0^2$ , where  $r$  and  $z$  are cylinder coordinates,  $W_0$  is the beam-waist radius, and  $\omega$  is the angular frequency of light. Quantities belonging to the forward beam (in positive  $z$  direction) are distinguished from those belonging to the backward beam (in negative  $z$  direction) by subscripts  $f$  and  $b$ , respectively.

Let  $F(\rho, \xi)$  be the electric field strength after separation of the factor  $\exp[i(kz - \omega t)]$ . We write the electric field strength in the continuous-wave regime as

$$E(\vec{r}, t) = F(\vec{r}) \exp[i(kz - \omega t)]. \quad (1)$$

In paraxial approximation, the equations for the functions  $F$  characterizing the forward- and the backward-propagating wave are then

$$\nabla_T^2 F_f(\rho, \xi) + 2i \partial_\xi F_f(\rho, \xi) = -\frac{\omega^2}{c^2} W_0^2 \left[ 1 + \frac{\alpha_f}{\epsilon_0} \right] F_f, \quad (2a)$$

$$\nabla_T^2 F_b(\rho, \xi) - 2i \partial_\xi F_b(\rho, \xi) = -\frac{\omega^2}{c^2} W_0^2 \left[ 1 + \frac{\alpha_b}{\epsilon_0} \right] F_b. \quad (2b)$$

The operator  $\nabla_T^2 = \partial_\rho^2 + \rho^{-1} \partial_\rho$  is the Laplacian in the transverse plane  $\xi = \text{const}$ .

On the right-hand side occurs the polarizability  $\alpha_{f,b}$  which, in the weak-gain approximation, consists of a

linear part and the saturation term which contains the intensities of the electric field. In a three-step procedure  $\alpha_{f,b}$  will be approximated by simpler expressions, better tractable in analytical and numerical calculations.

*Step 1.* We recall that both the linear polarizability and the coefficients of the electric field intensities in the saturation term are proportional to the population difference between higher and lower energy states [see Ref. 37, Eqs. (A2), (A15), (A16), (A22), and (A23)]. In terms of its on-axis value  $N_0$  this number is given by

$$N = N_0(1 - u\rho^2) = N_0(1 - r^2/r_0^2),$$

where  $u$  is a dimensionless parameter depending, e.g., on the diameter of the tube.

At a point  $(\rho, \xi)$  the polarizability in the forward and backward beams can thus be written in the form

$$\alpha_f(\rho, \xi) = [\alpha_0 + \beta_1 |E_f(\rho, \xi)|^2 + \beta_2 |E_b(\rho, \xi)|^2] (1 - u\rho^2), \quad (3a)$$

$$\alpha_b(\rho, \xi) = [\alpha_0 + \beta_2 |E_f(\rho, \xi)|^2 + \beta_1 |E_b(\rho, \xi)|^2] (1 - u\rho^2). \quad (3b)$$

The approximation (step 1) consists in assuming that the coefficients  $\alpha_0$ ,  $\beta_1$ , and  $\beta_2$  take the same values at any point in the tube. They are determined by atomic data of the active medium. Expressions for them can be found in Ref. 37 (where  $\beta_1$  and  $\beta_2$  had been named  $\alpha_1$  and  $\alpha_2$ ). The coefficient  $\beta_1$  takes care of the self-saturation of a wave, whereas  $\beta_2$  is responsible for the saturation by an oncoming wave, a phenomenon from which the Lamb dip originates. The analysis of the two parameters shows the form of the sub-Doppler line.<sup>36</sup>

*Step 2.* In the saturation term the field intensities are assumed to have the transverse shape given by a Gaussian, i.e., the same  $\rho$  dependence as one would find in a passive cavity. This assumption gives

$$|E(\rho, \xi)|^2 = |E(0, \xi)|^2 \exp\left[-2 \frac{W_0^2}{W^2} \rho^2\right]. \quad (4)$$

*Step 3.* We consider the dependence of the nonlinear part of the polarizability on the radial coordinate  $\rho$  which is of the form

$$(1 - u\rho^2) \exp\left[-2 \frac{W_0^2}{W^2} \rho^2\right].$$

In any transverse section we approximate this form by a parabola  $1 - A(\xi)\rho^2$ . Each parabola may be visualized as the transverse cut of a two-dimensional coaxial surface whose equation is  $\rho = \bar{\rho}W/W_0$ ,  $\bar{\rho}$  being a (positive) constant. This means that we define a function  $A(\xi)$  by demanding that the condition

$$(1 - u\rho^2) |E_f(\rho, \xi)|^2 = (1 - A(\xi)\rho^2) |E_f(0, \xi)|^2$$

is satisfied on the surface  $\rho = W\bar{\rho}/W_0$ . With (4) we get

$$A(\xi) = \frac{\bar{\rho}^{-2}}{1 + 4\xi^2} + \left[ u - \frac{\bar{\rho}^{-2}}{1 + 4\xi^2} \right] \exp(-2\bar{\rho}^2). \quad (5)$$

In these equations  $W(\xi)$  represents the beam radius of a

fundamental Gaussian mode. We recall the relation  $(W/W_0)^2 = 1 + 4\xi^2$ . The constant  $\bar{\rho}$  is a positive parameter whose upper bound is determined by the condition that the surface on which the equality holds lies inside the tube. Figure 1 shows the function

$$\frac{(1 - u\rho^2) \exp[-2\rho^2/(1 + 4\xi^2)]}{1 + 4\xi^2}$$

together with the approximating parabola for the value  $u = 8.8 \times 10^{-3}$  in one laser we are using in our experiment (to be described in Sec. III). The description of the saturated medium has been simplified since, e.g., neither the spatial harmonics (saturation gratings) nor the variation of the collision parameters as a function of intensity have been taken into account.

The nonuniform parts of the polarizability of the forward and backward waves can now be written as

$$\alpha_{nf} = \epsilon_0 T_f(\xi) - \rho^2 [u\alpha_0 + A\epsilon_0 T_f(\xi)], \quad (6a)$$

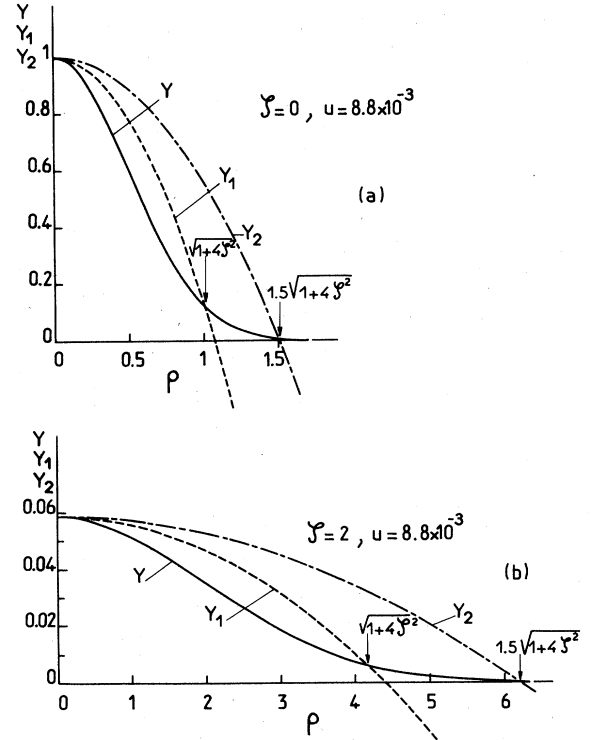


FIG. 1. Illustration of the parabolic approximation of the function  $Y = (1 - u\rho^2) \exp[-2\rho^2/(1 + 4\xi^2)] / (1 + 4\xi^2)$ . Solid curve: function  $Y$ . Dashed curve: parabola  $Y_1 = 1 - A(\xi)\rho^2$  with  $\bar{\rho} = 1$  in  $A(\xi)$  [see Eq. (5)]. Dot-dashed curve: parabola  $Y_2 = 1 - A(\xi)\rho^2$  with  $\bar{\rho} = 1.5$ . These curves have been calculated for a quasi-hemispherical cavity 57 cm long with a concave mirror having a radius of curvature  $R = 60$  cm. In this case  $W_0 = 0.376$  mm on the plane mirror where  $\xi = 0$ .  $\rho$  is the scaled transverse coordinate such that  $\rho = r/W_0$ . Two values of the scaled longitudinal coordinate  $\xi = \lambda z / 2\pi W_0^2$  have been used:  $\xi = 0$  in (a) and  $\xi = 2$  in (b) corresponding to  $z = 523$  mm near the concave mirror. The value  $u = 8.8 \times 10^{-3}$  has been used in  $A(\xi)$ . These curves show that  $A(\xi)$  ensures the same approximation for  $y$  along the entire length of the laser. They also illustrate the spreading of intensity as shown by the different scales in (a) and (b).

$$\alpha_{nb} = \epsilon_0 T_b(\xi) - \rho^2 [u \alpha_0 + A \epsilon_0 T_b(\xi)], \quad (6b)$$

where we have introduced the auxiliary functions of a single variable:

$$\epsilon_0 T_f(\xi) := \beta_1 |E_f(0, \xi)|^2 + \beta_2 |E_b(0, \xi)|^2, \quad (7a)$$

$$\epsilon_0 T_b(\xi) := \beta_2 |E_f(0, \xi)|^2 + \beta_1 |E_b(0, \xi)|^2. \quad (7b)$$

The important result of the three-step procedure is the expressions (6a), (6b) for the nonlinear part of the polarizability showing that in this approximation the response of the medium is summarized by a quadratic-complex index which varies along the axis.

We consider now a passive cavity in single-mode operation. It is well known that the corresponding field is the "fundamental Gaussian"

$$F_0 = (q_0/q) \exp(-\rho^2 q_0/q) \quad (8)$$

whose curvature is given by  $q/q_0 = 1 + 2i\xi$ . The beam waist is located at  $\xi_0$  and its radius  $W_0$  is related to the curvature by  $kW_0^2 = 2iq_0$ . The parameters  $\xi_0$  and  $W_0$  are determined by the radii of curvature and the location of the mirrors via the boundary conditions. The usual convention is to put the origin of the  $\xi$  axis at the beam waist,  $\xi_0 = 0$ . At an arbitrary position  $\xi$  the beam diameter  $2W$  is given by the formula  $(W/W_0)^2 = 1 + 4\xi^2$ . The backward beam corresponding to expression (8) is obtained by taking the complex conjugate.

If a medium (laser active or not) is introduced into the cavity, the beam will generally lose its property of being Gaussian. However, if the medium can be described by a quadratic index (which is a complex function), the deformed beam will also be Gaussian, though with another curvature, denoted by  $\tilde{q}$ .

We define the transverse beam parameter variations for the forward and backward beams by

$$\eta_f = 2iq_0(1/\tilde{q}_f - 1/q_f), \quad (9)$$

$$\eta_b = 2iq_0(1/\tilde{q}_b - 1/q_b).$$

In order that the deformed beam is Gaussian again, the two complex functions have to satisfy the nonlinear differential equations

$$\eta'_f + \frac{4i}{1+2i\xi} \eta_f + \eta_f^2 = -\frac{\omega^2}{c^2} W_0^2 \left[ \frac{\alpha_0}{\epsilon_0} u + AT_f \right], \quad (10a)$$

$$\eta'_b - \frac{4i}{1-2i\xi} \eta_b + \eta_b^2 = -\frac{\omega^2}{c^2} W_0^2 \left[ \frac{\alpha_0}{\epsilon_0} u + AT_b \right]. \quad (10b)$$

The equations are independent of each other. Their solutions, however, are coupled by the boundary conditions which are to be imposed at  $\xi_1$  and  $\xi_2$ , the sites of the mirrors. These boundary conditions are

$$(\eta_f + \eta_b)_{\xi_1} = 0, \quad (\eta_f + \eta_b)_{\xi_2} = 0. \quad (11)$$

The field in the presence of the medium will be given by

$$F_f(\rho, \xi) = F_{f0}(\rho, \xi) \exp[-i(\epsilon_f - \frac{1}{2}\rho^2 \eta_f)], \quad (12a)$$

$$F_b(\rho, \xi) = F_{b0}(\rho, \xi) \exp[-i(\epsilon_b + \frac{1}{2}\rho^2 \eta_b)], \quad (12b)$$

with functions  $\epsilon_f$  and  $\epsilon_b$  which have to satisfy the differential equations

$$\epsilon'_f + i\eta_f = -\frac{1}{2} \frac{\omega^2}{c^2} W_0^2 T_f, \quad (13a)$$

$$\epsilon'_b + i\eta_b = \frac{1}{2} \frac{\omega^2}{c^2} W_0^2 T_b. \quad (13b)$$

It is seen from (12) that the two complex functions  $\epsilon_f$  and  $\epsilon_b$  represent that modification of amplitude and phase in the beam which is independent of the transverse coordinate  $\rho$ . In many applications the variations of the transverse beam parameters furnish enough information about the laser beam geometry that one does not have to know  $\epsilon_f$  and  $\epsilon_b$ . However, if one needs these functions their boundary values have to be found. They are obtained from the conditions that first, the losses (e.g., on the mirrors) are compensated by the gain and second, the optical length of the cavity has to be a multiple of the semiwavelength  $\lambda/2$ .

In this section we are using the linearized version of the beam parameter variation equation (10) whose right-hand side is approximated by a polynomial of second degree in the function  $(W_0/W)^2$ . This equation has already been motivated, discussed, and solved in previous work.<sup>32,33</sup> Here we need the solution for a quasi-semihemispheric cavity with the plane mirror at  $\xi=0$ , the concave mirror at  $\xi_2$ , and the tube between  $\xi_3$  and  $\xi_4$ . The beam parameter variation  $\eta_{f2}$  at the concave mirror ( $\xi=\xi_2$ ) is found to be

$$\eta_{f2} = -i \frac{\omega^2}{c^2} W_0^2 \frac{(1+4\xi_4^2)^2}{4\xi_2} \times \left[ \frac{\alpha_0}{\epsilon_0} C_p + E_0^2 \frac{\beta_1 + \beta_2}{\epsilon_0} (C_m + C_s) \right]. \quad (14)$$

We have set  $|E_{0f}|^2 = |E_{0b}|^2 =: E_0^2$  (cf. Ref. 33, p. 3454),

$$C_p = \frac{u}{3} [\xi_4(4\xi_4^2 - 3) - \xi_3(4\xi_3^2 - 3)],$$

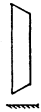

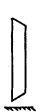
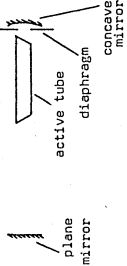
$$C_m = u \exp(-2\bar{\rho}^2) (\xi_4 - \xi_3 + \arctan 2\xi_3 - \arctan 2\xi_4),$$

$$C_s = \frac{1 - e^{-2\bar{\rho}^2}}{\bar{\rho}^2} \left[ \frac{\xi_3}{1+4\xi_3^2} - \frac{\xi_4}{1+4\xi_4^2} \right].$$

The three real coefficients  $C_p$ ,  $C_m$ , and  $C_s$  are largely of geometrical nature, depending on the positions of optical components in the cavity.  $C_p$  and  $C_s$  belong, respectively, to the terms of population and saturation.  $C_m$  belongs to a term where both population and saturation influence are mixed. We are introducing these quantities only for reasons of convenience.

The beam parameter variation  $\eta$  represents the change of the curvature parameter caused by the optical action of the medium. In order to know the corresponding change of the beam width and the curvature of the wave fronts we have to calculate the real and imaginary part of  $\eta$ . We indicate them by superscripts  $r$  and  $i$ . The imaginary part is related to the change of the beam radius by  $\delta W/W^3 = -\eta^i/4W_0^2$ . On the concave mirror we have

TABLE I. Values of the geometric coefficient  $C_s, C_p, C_m$  (see definition in text) for the four studied experimental configurations. Two discharge tubes are used: The first is 8 mm in internal diameter and has a weaker population inhomogeneity than the second, which is narrower (bore 4 mm). Each tube can be displaced inside the resonator which consists of a plane and a concave mirror (radius of curvature: 60 cm) separated by 57 cm. Results described below are obtained for the indicated values of  $z_3$  and  $z_4$  which correspond to positions of the tubes near the plane mirror (configurations 1 and 3) and near the concave mirror (configurations 2 and 4). These two positions permit varying the inhomogeneity of saturation while the two tubes permit varying the inhomogeneity of population. The dominant inhomogeneity is deduced in comparing numerical values of  $C_p$  and  $C_s$  ( $C_m$  is always smaller). However, comparison with experimental and numerical results described in Sec. III show that  $C_s$  is underestimated in the model used here.

	Experimental configuration	Endpoints of active column	Geometric coefficients (calculated with $\bar{p}=1$ )	Dominant inhomogeneity	Type of asymmetry
Tube 1		$z_3=28$ mm $z_4=248$ mm	$r_0=4$ mm $C_p=2.6 \times 10^{-3}$ $C_m=-4.0 \times 10^{-5}$ $C_s=-9.0 \times 10^{-2}$	Saturation	If
Internal diameter 8 mm Active length 220 mm		$z_3=322$ mm $z_4=542$ mm	$r_0=4$ mm $C_p=7.5 \times 10^{-2}$ $C_m=8.3 \times 10^{-4}$ $C_s=5.2 \times 10^{-2}$	Competition	hf if saturation effects dominate
Tube 2		$z_3=17$ mm	$r_0=2.5$ mm $C_p=-1.3 \times 10^{-3}$ $C_m=-4.6 \times 10^{-4}$ $C_s=-1.4 \times 10^{-1}$	Saturation	If increasing with current
Internal diameter 4 mm Active length 191 mm		$z_4=208$ mm $z_3=356$ mm $z_4=547$ mm	$r_0=3$ mm $C_p=-9.4 \times 10^{-4}$ $C_m=-3.2 \times 10^{-4}$ $C_s=-1.4 \times 10^{-1}$	Population	If at low currents Decreasing at high currents

$$\delta W/W^3 = \frac{\omega^2 (1+4\xi_4^2)^2}{c^2 16\xi_2} \left[ \frac{\alpha_0^r}{\epsilon_0} C_p + E_0^2 \frac{\beta_1^r + \beta_2^r}{\epsilon_0} (C_m + C_s) \right]. \quad (15)$$

One notes that the variation of  $W$  is dispersion shaped. This is not the case everywhere inside the cavity because, in general, the geometric factor of  $\alpha_0$  (or  $\beta_1$  and  $\beta_2$ ) is complex [see Eq. (22) of Ref. 32].

The variation of  $W$  has an effect on the output intensity of the laser (Garside effect<sup>23</sup>): If  $W$  decreases ( $\delta W < 0$ ), diffraction losses are weaker and the field intensity is stronger. In order to see the predictive power of the above formula and the validity of the model leading to it, we have numerically calculated the various coefficients appearing in (15) for the experimental cases described below (Table I). For instance, if we find that the term  $C_p$  is positive and greater than the terms  $C_m$  or  $C_s$ , we conclude that  $\delta W$  will have a dispersion shape fixed by  $\alpha_0^r$ , with the maximum on the high-frequency side. Consequently, the diffraction losses will be maximal on this side, causing the maximum of intensity to be on the side of low frequencies (lf type). Table I shows various situations leading to vari-

ous asymmetries. Experiments described in the next paragraph show good agreement with predictions obtained from the above formula, though the saturation term has been underestimated. Comparison with numerical results (where terms  $\eta_b^2$  and  $\eta_f^2$  were included) also shows satisfactory agreement. One may conclude that formula (15) together with the Garside effect can give a good qualitative prediction of the type of asymmetry.

The real part of the beam parameter variation is related to the variation of the curvature of wave fronts in the forward beam by  $\delta(1/R_f) = c\eta_f^r/\omega W_0^2$ . We find on the concave mirror

$$\delta(1/R_f) = \frac{\omega (1+4\xi_4^2)^2}{c 4\xi_2} \left[ \frac{\alpha_0^i}{\epsilon_0} C_p + E_0^2 \frac{\beta_1^i + \beta_2^i}{\epsilon_0} (C_m + C_s) \right]. \quad (16)$$

At that point of the laser, the variation of curvature is absorption shaped. Since  $\alpha_0^i$  is negative we have  $\delta(1/R_f) < 0$  in the case where the population term is dominant. This fact is confirmed by the numerical results given in the next section.

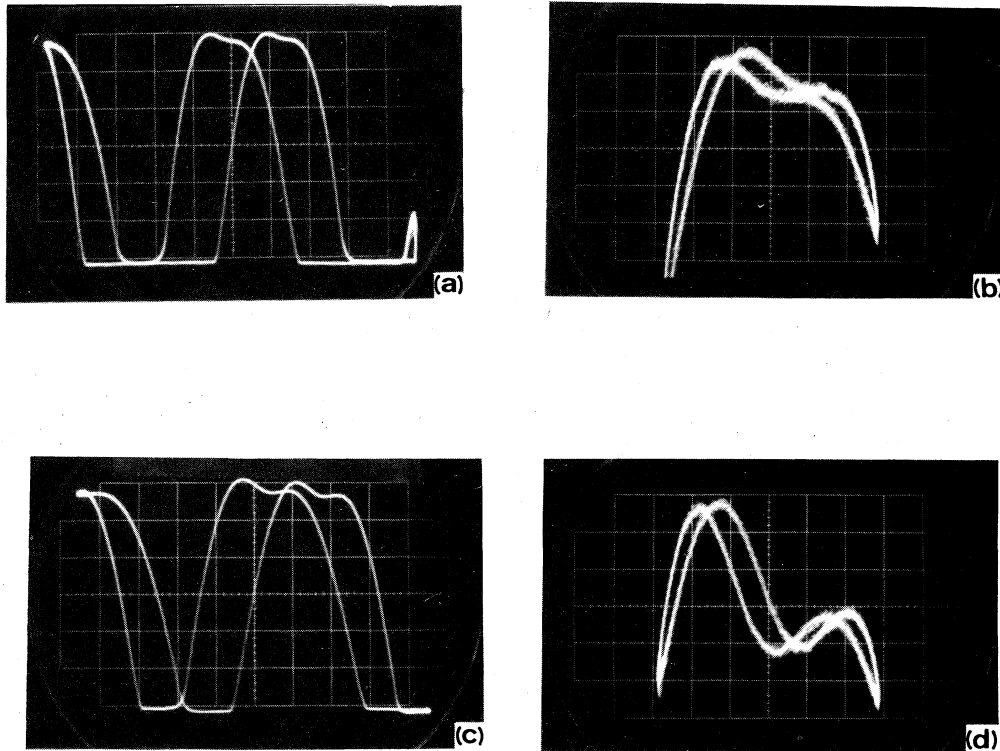


FIG. 2. Laser output vs frequency for configuration 1 of Table I (tube 1 on plane-mirror side). Intensities are in arbitrary units. Frequencies increase from left to right. For the cavity used,  $c/2d = 263$  MHz indicating that a division on the horizontal scale is 45 MHz [in (a) and (c)]. Doubling and deformation of the curves result from hysteresis and nonlinearity effects of the piezoelectric ceramic. (a) and (c) show entire line shapes while (b) and (d) are magnifications of Lamb-dip regions [ $X \times 2.5$  and  $Y_{(a)} \times 5$  for (b) and  $Y_{(c)} \times 10$  for (d)]. A diaphragm 3.5 mm in diameter is set on the concave mirror and this feature is the same for the other experimental results given in this paper. Results are shown for two values of the discharge current:  $i_c = 11$  mA [in (a) and (b)] and  $i_c = 13.5$  mA [in (c) and (d)] where intensity is two times greater. The asymmetry of the line is of lf type. It is due to saturation inhomogeneity and increases linearly with intensity. The factor of asymmetry as defined by Freed and Haus (Ref. 21) is  $f = 2(H-h)/(H+h)$ , where  $H$  and  $h$  are, respectively, the intensities at lf and hf maximum. In (a),  $f = 2.2\%$ , in (b),  $f = 4.2\%$ .

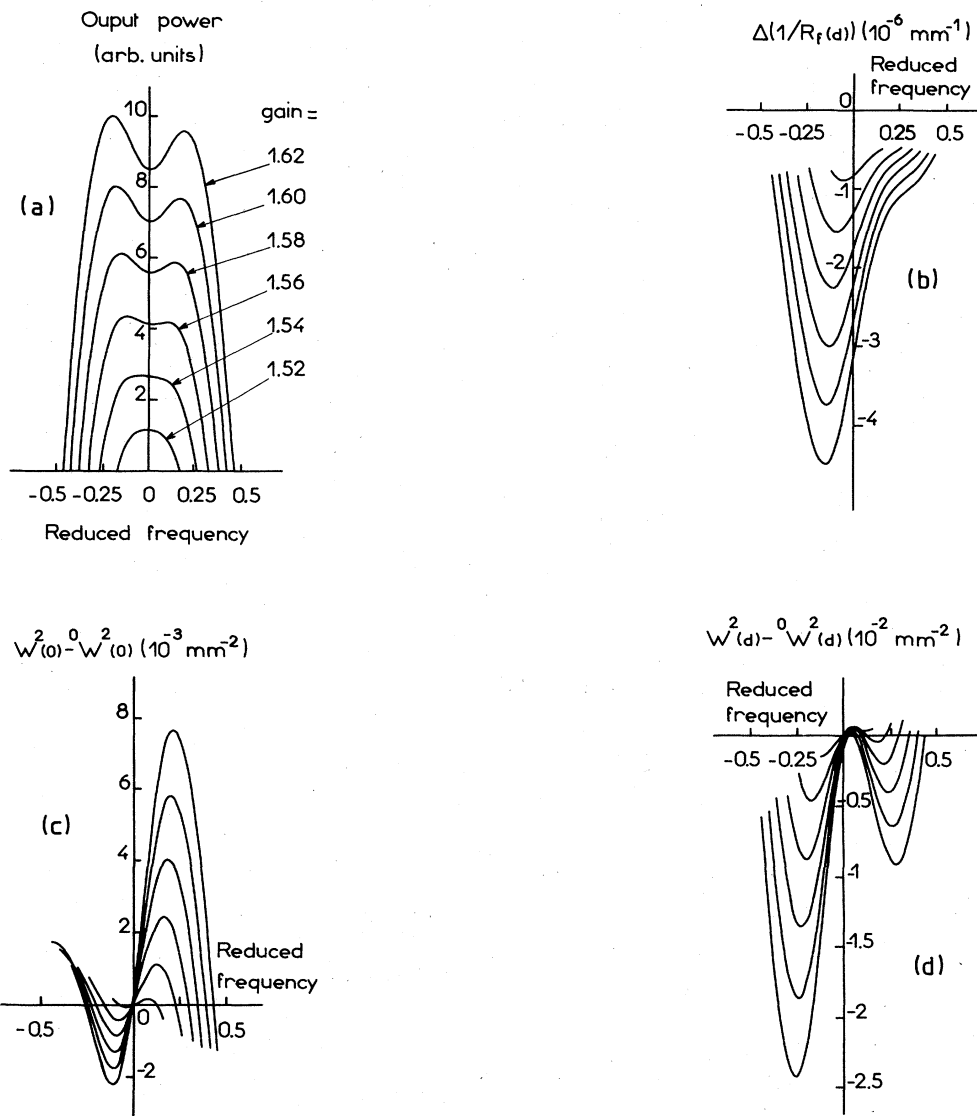


FIG. 3. Theoretical curves calculated by the method described in Ref. 32 and using numerical integration of nonlinear equations (10). These curves are calculated for six values of the gain, as indicated on (a), and for configuration 1 of Table I. The value of the imaginary part of the complex argument of the plasma dispersion function is chosen to be 0.2. (a) shows the output power vs frequency detuning. The maximum of intensity is on the low-frequency side of the line and the Lamb dip is blue shifted. This lf-type asymmetry increases with intensity in good agreement with experiment (Fig. 2). (b) shows the variation of the curvature  $R_f^{-1}(d)$  of the forward beam on the concave mirror. One notes that  $\Delta[1/R_f(d)] < 0$  in agreement with prediction of formula (16) where the factor of  $|E_0|^2$  is negative. Because  $C_p = 2.6 \times 10^{-3}$  is positive, the population factor is also negative (remember  $\alpha_0^i < 0$  and  $\beta_1^i$  and  $\beta_2^i > 0$ ). However, absorption-shaped curves predicted by Eq. (16) are strongly deformed by amplification effects. (c) and (d) show the variations of  $W^2$  on the plane (c) and concave mirrors (d). When a diaphragm is set on this mirror, (d) shows that diffraction losses are lower on the low-frequency side giving a lf-type asymmetry of the line via Garside's effect. (c) also predicts the same type of asymmetry when the diaphragm is placed on the plane mirror; we have also experimentally verified this prediction. One notes that (d) disagrees with formula (15) which is based on the simple Gaussian linear model and which predicts dispersion-shaped curves.  ${}^0W_{(0)}^2$  and  ${}^0W_{(d)}^2$  are the unperturbed values for the empty cavity on the plane and concave mirrors.

### III. EXPERIMENTAL RESULTS

For the experimental verification of our previous results we have used a quasihemispheric resonator with a concave mirror of radius of curvature  $R = 60$  cm and a length of  $d = 57$  cm. Reflectances of plane and concave mirrors were 0.90 and 0.64, respectively, for  $\lambda = 3.39 \mu\text{m}$ . A dia-

phragm of 3.5 mm in diameter was placed on the concave mirror. With this geometry the beam radius is  $W_0 = 0.376$  mm at the plane mirror and  $W_d = 1.68$  mm at the concave mirror. The strong variation ( $W_d/W_0 = 4.5$ ) of the radius of the mode between the two mirrors allows us to test the respective influences of the inhomogeneities of population and saturation by displacing a tube of

length 20 cm inside the resonator. When the tube is placed near the concave mirror where the beam width is large, the light will "probe" the inhomogeneity of population over a wider range of the transverse distance. The population inhomogeneity will, therefore, have a greater influence on the line shape. In the other experiment, the tube is placed on the side of the plane mirror where the beam width is small. In this case it is expected that the saturation inhomogeneity is predominant.

The experimental results given below show the spectrum of the output intensity at the curved mirror as a function of the resonator length for different values of the discharge current. We also show enlargements of the Lamb-dip sections. The doubling of the curves is due to the hysteresis of the piezoelectric ceramic. The laser is in monomode operation as shown by the fact that the intensity is zero between two successive modes. The theoretical curves are obtained by our previous method,<sup>32</sup> but using the full nonlinear equations for  $\eta$  [i.e., Eqs. (10)]. We picture the variations of the diameter of the mode on both mirrors, the variation of the wave-front curvature of the forward beam, and the output intensity at the curved mirror ( $\xi_2$ ) for six different values of the gain. We have used  $\bar{\rho}=1.5$ .

The first tube we used has an inner diameter of 8 mm (corresponding to  $r_0=4$  mm) and a length of 22 cm. We recall here that  $r_0$  is that value of the transverse coordi-

nate for which the number density of the inverted population becomes zero. We have  $u=(W_0/r_0)^2$  which gives in our case  $u=8.8\times 10^{-3}$ . The inhomogeneity of population is weak. The pressure is 0.6 mm Hg (0.1 Torr for  $^{20}\text{Ne}$ , 0.5 Torr for He).

Figure 2 represents the measured line shapes when the amplifying tube is on the side of the plane mirror (configuration 1 of Table I). They are given for two values of the discharge current,  $i=11$  and 13.5 mA. The line is strongly asymmetric of the hf type (maximum on the low-frequency side), and the asymmetry increases with the discharge current. This is in agreement with our interpretation: The asymmetry results here from the saturation effects which increase with intensity. One notes that the minimum of the line is displaced towards higher frequencies. The corresponding numerical results [Fig. 3(a)] are in agreement with both the measured line shape and the predictions of the Gaussian beam model.

Figures 3(c) and 3(d) show the variation of the spot size on the plane mirror and the concave mirror. The influence of diffraction and amplification, which change the distribution of the field in the laser, results in a strong modification of the dispersion curve predicted by Eq. (15). Moreover, a look at Fig. 3(d) shows, in view of the Gar-side effect,<sup>23</sup> that the losses due to diffraction are smaller on the low-frequency side, in agreement with the measured line shape (Fig. 2). A diaphragm placed on the

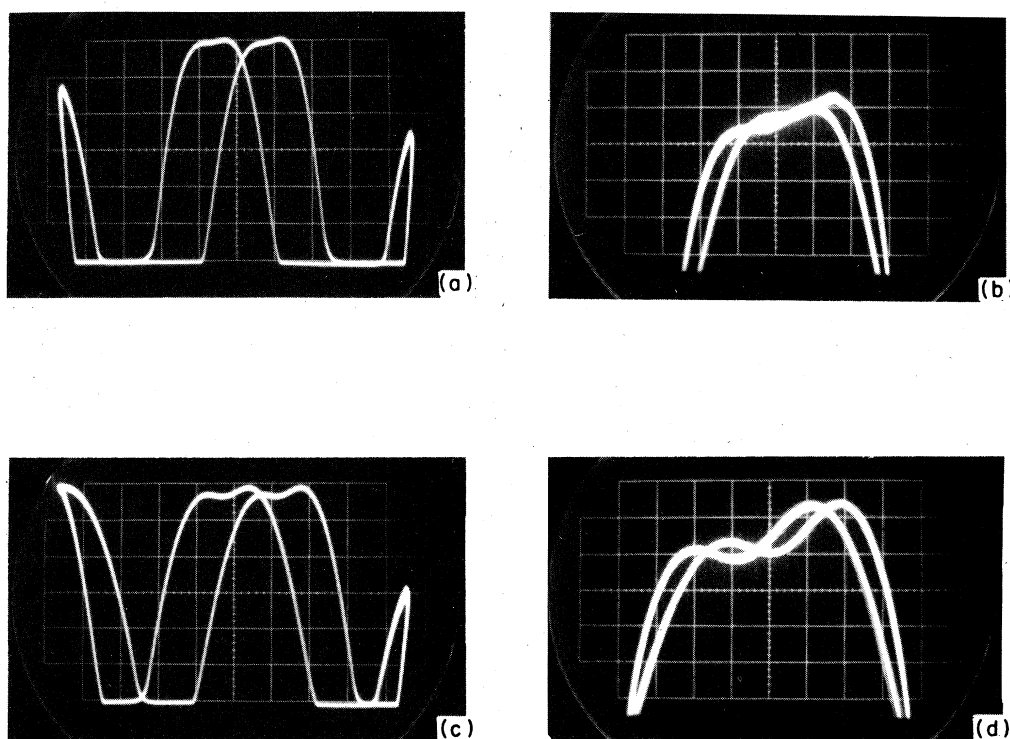


FIG. 4. Experimental line shapes obtained when tube 1 (large bore) is placed on the concave-mirror side (configuration 2 of Table I). Discharge currents are 11 mA [in (a) and (b)] and 13.5 mA [in (c) and (d)]. Intensities are about five times greater than those given in Fig. 2. Magnification factors are  $X\times 2.5$  and  $Y\times 5$  for (b) and (d). Intensity is two times greater in (c) than in (a). The lines show a hf type of asymmetry due to saturation. We find  $f=1.6\times 10^{-2}$  in (a) and  $f=3.5\times 10^{-2}$  in (c). In this configuration, pumping of energy is much more efficient than in the previous experiment because the volume of the mode is greater. This is why the saturation effect becomes greater than the population one.



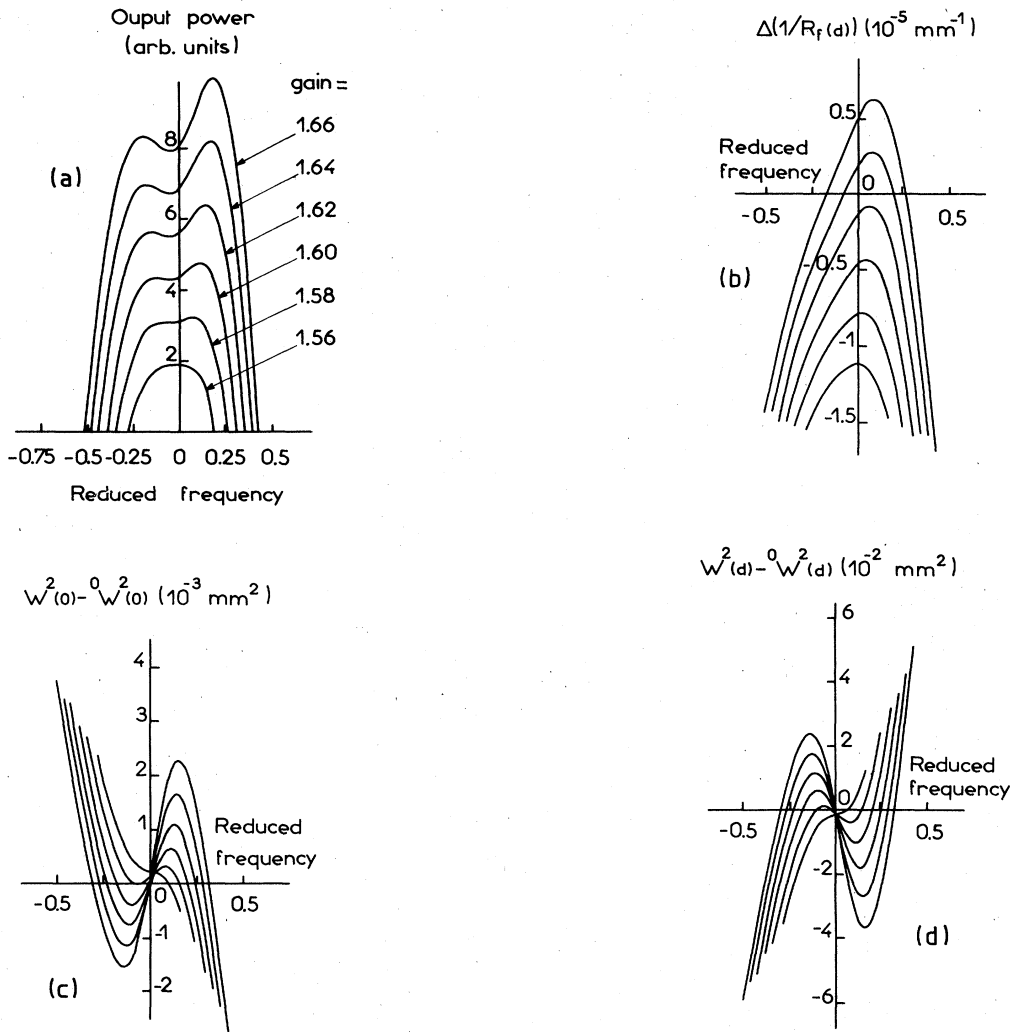


FIG. 5. Theoretical curves corresponding to the experiment leading to Fig. 4 and to configuration 2 of Table I. (a) shows a prominent asymmetry of the hf type and a red-shifted Lamb dip in agreement with experimental curves of Fig. 4. (b)–(d) show the competition between population and saturation effects. In (b) saturation effects alone would give positive values [the factor of  $|E_0|^2$  is positive in (16)] but population effects shift the curves downward. In (d) one sees that the curves result from the superposition of two dispersion-shaped functions. The first one has its maximum on the low-frequency side and is due to the saturation effect [the factor of  $\beta_1 + \beta_2$  is positive in (15)] and the second one has its minimum on this side and is due to the population effect [the factor of  $\alpha_0^2$  is also positive in (15)]. The same phenomenon, but with a reverse sign, is noticeable in (c). We have verified that it can be predicted from a formula analog to (15) but calculated for  $\zeta=0$  from Eq. (22) of Ref. 33. We have also experimentally verified that a diaphragm placed on the plane mirror leads to a line with an asymmetry of the lf type, contrary to that of (a). As in Figs. 2(c) and 2(d), one sees that the variation of  $W^2$  does not vanish at line center, contrary to the prediction of Eq. (15). This is because we have used the nonlinear Eq. (10) for our numerical calculation. The term  $\eta^2$  is then responsible for this discrepancy, and this is its main effect.

plane mirror will result in a similar line shape since the minimum of  $\Delta W_0^2$  is also on the low-frequency side. Figure 3(b) shows the variation of the inverse radius of curvature,  $\Delta(1/R_f)$ , of the forward beam on the concave mirror. One notes good agreement between the observed sign ( $\Delta[1/R_f(d)] < 0$ ) of the variation and the prediction of the calculation [Eq. (16)]. The quantity  $\Delta[1/R_f(d)]$  is mainly determined by the negative saturation term.

Figure 4 shows the measured line shapes (tube near the concave mirror) for the same values of the discharge current as before. One notes that the asymmetry is of the

high-frequency (hf) type and that it increases with the gain (i.e., the saturation), in agreement with the predictions of Table I. This time the minimum of the Lamb dip is found on the low-frequency side.

Figure 5(a) pictures the line shapes obtained by numerical calculation for the same value of the parameter ( $r_0=4$  mm) as before. Comparing it with Fig. 3(a), one notices a rather spectacular change in the type of the asymmetry. Figures 5(c) and 5(d) show the variations of the spot size on the mirrors. We note the appearance of two important phenomena. First, near the center of the line, one ob-

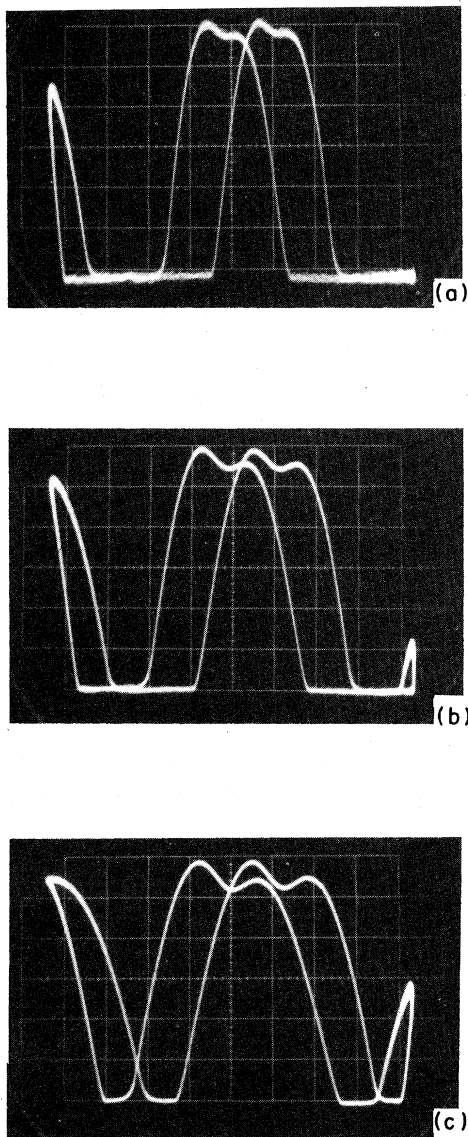


FIG. 6. Experimental line shapes obtained when the narrow amplifying tube is on the side of the plane mirror (configuration 3 of Table I). Discharge currents are  $i_c = 4.5$  mA (a),  $i_c = 5$  mA (b), and  $i_c = 6$  mA (c). While currents are lower, densities are stronger in this tube than in the other. Intensity in (c) is two times that of (b) which is also two times that of (a). Asymmetries are of the lf type as in configuration 1 (Fig. 2) but more pronounced due to a greater gain coming from the greater density of the discharge current. In (a),  $f = 3.2 \times 10^{-2}$ ; in (b),  $f = 5.2 \times 10^{-2}$ ; and in (c),  $f = 7.2 \times 10^{-2}$ , showing that the asymmetry does not increase linearly with intensity.

serves that  $\Delta W_d^2$  [Fig. 5(d)] decreases towards higher frequencies, which leads to an asymmetry of the hf type. The second phenomenon is due to the inhomogeneity of population which enhances  $\Delta W_d^2$  on the hf side and diminishes it on the lf side. A similar situation exists in the the outer regions of the line, i.e., at very low intensities,

where the variation of the diameter of the mode does not vanish. The described phenomena are also present at the plane mirror [Fig. 5(c)], however, for  $\Delta W_0^2$ , in the opposite sense. Comparing Figs. 3(c) and 3(d) with 5(c) and 5(d) one observes that the influence of the population inhomogeneity is more sensible in the latter case because of the larger width of the mode. Despite this fact, it does not show in the line shape. The variation of the curvature  $1/R$  of the forward beam is pictured in Fig. 5(b). One notices a change as compared to the preceding case [Fig. 3(b)]. The value of  $\Delta[1/R_f(d)]$  is negative at weak intensities (then it must depend essentially on  $C_p > 0$ ); with increasing intensity the term  $C_s$  becomes more important and pushes the curves upward.

The experiments pictured in Figs. 2–5 show that in the case of the wider tube it is essentially the inhomogeneity of saturation which fixes the line shape through the  $R$  effect<sup>27</sup> which adds to the Garside effect. The distribution of the resonant diffracted field influences the sense of the asymmetry of a line.<sup>34</sup> The population inhomogeneity, though weak in this case, influences the evolution of the diameter of the mode as well as the variation of the beam curvature, especially when the amplifying tube is on the side of the concave mirror.

We now turn to measured data obtained with the second tube, which has an internal diameter of 4 mm, a length of 190 mm, and a pressure of 0.5 Torr (0.1 Torr of  $^{20}\text{Ne}$ ). In this case we have a maximal value of  $u = 0.0353$  for  $r_0 = 2$  mm. As the diameter of the tube is smaller than before, one can predict that an increase of the discharge current will give rise to a decrease of  $u$  (the distribution of population becomes flatter).

Figure 6 represents the measured line shapes when the tube is on the side of the plane mirror. These curves, as those of Fig. 2, show an asymmetry of the low-frequency type caused by the inhomogeneity of saturation.

The curves picturing output intensities, variations of spot size, and beam curvature, Figs. 7(a)–7(d), have been calculated for a parameter value  $r_0 = 2.5$  mm. These curves correspond to those of Figs. 3(a)–3(d). Changing the diameter of the tube does not result in new line shapes [see Fig. 7(a)], simply because the diameter of the mode is small ( $2W_0 = 0.75$  mm) in that region and the field does not “probe” very much the population inhomogeneity. In contrast, one notes an influence on the values of  $\Delta W_0^2$  [Fig. 7(c)] and  $\Delta W_d^2$  [Fig. 7(d)] which are not canceled by the intensity in the outer regions of the line, due to the term  $\alpha'_0/\epsilon_0$ . This influence is likewise found when Figs. 7(d) and 3(d) are compared, indicating a strong variation on the hf side. The difference between these curves and those predicted by the preceding formula is due to the difference between the amplitude of the Gaussian field and that of the diffracted field, the latter of which includes the focalizing power of the diaphragm<sup>34</sup> and which is taken care of in the numerical calculations.

Figure 8 represents the measured line shapes when the tube is on the side of the concave mirror. One notes that the type of asymmetry changes when the discharge current is increased: At weak currents ( $i = 7$  mA) the asymmetry is of the lf type which, as the current is increased, is gradually transformed into the hf-type asym-

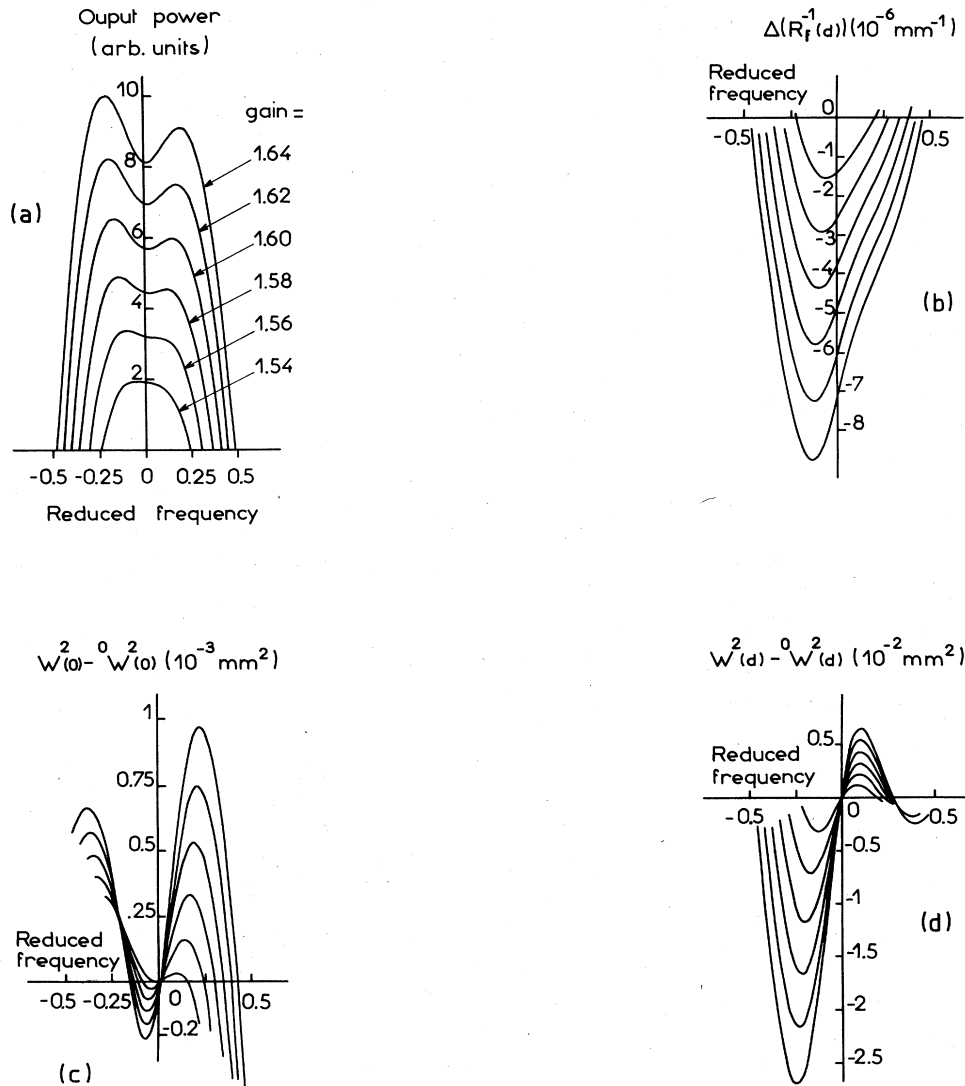


FIG. 7. Theoretical results corresponding to configuration 3 of Table I. Calculation has been made with  $u$  corresponding to  $r_0 = 2.5$  mm, i.e.,  $u = 2.6 \times 10^{-2}$ . Comparison with results of configuration 1 (Fig. 3) shows no new feature on the line shape (a); the asymmetry is of the lf type with a blue-shifted Lamb dip. However, an increase of  $u$  results in an upward shift of the curves (b) [compare with Fig. 3(b)] and a slight modification of the variation of  $W^2$ . The passage from negative to positive values of  $\Delta[W^2(d)]$  on the hf side [see Figs. 3(d) and 7(d)] is due to the different values of  $z_3$  (28 mm and 17 mm) used in the experiment.

metry, a phenomenon which we have already observed and discussed.<sup>34</sup> The explanation is based on the competition between the population and the saturation effect. At weak intensities the population term prevails. With increasing current the population inhomogeneity decreases while the inhomogeneity of saturation increases (because the intensity increases with the overall increasing gain due to increasing current) until the latter takes over and changes the type of asymmetry.

In order to see the influence of a slight change of  $u$  on line shapes, we have made the same calculation as before, but this time with two values of  $u$ . Figure 9 shows theoretical results with  $u = 2.26 \times 10^{-2}$  ( $r_0 = 2.5$  mm) and Fig. 10 with  $u = 1.57 \times 10^{-2}$  ( $r_0 = 3$  mm). Figure 9(a)

shows clearly the role of a strong population inhomogeneity effect in the formation of this line shape. The entire line is red shifted, the Lamb-dip asymmetry being of the lf type. The curves in Figs. 9(b)–9(d) are essentially shaped by population effects. These results agree with those of Table I.

Figure 10(a) reveals a spectacular change of the asymmetry of the line which comes with an unusual phenomenon: Here the minimum of the Lamb dip stays on the low-frequency side, though usually it is found on the side of the lower local maximum of the intensity. Comparing this situation with Figs. 5(a) and 9(a) where the population inhomogeneities are different, we conclude that the latter fix on asymmetry of the lf type which is

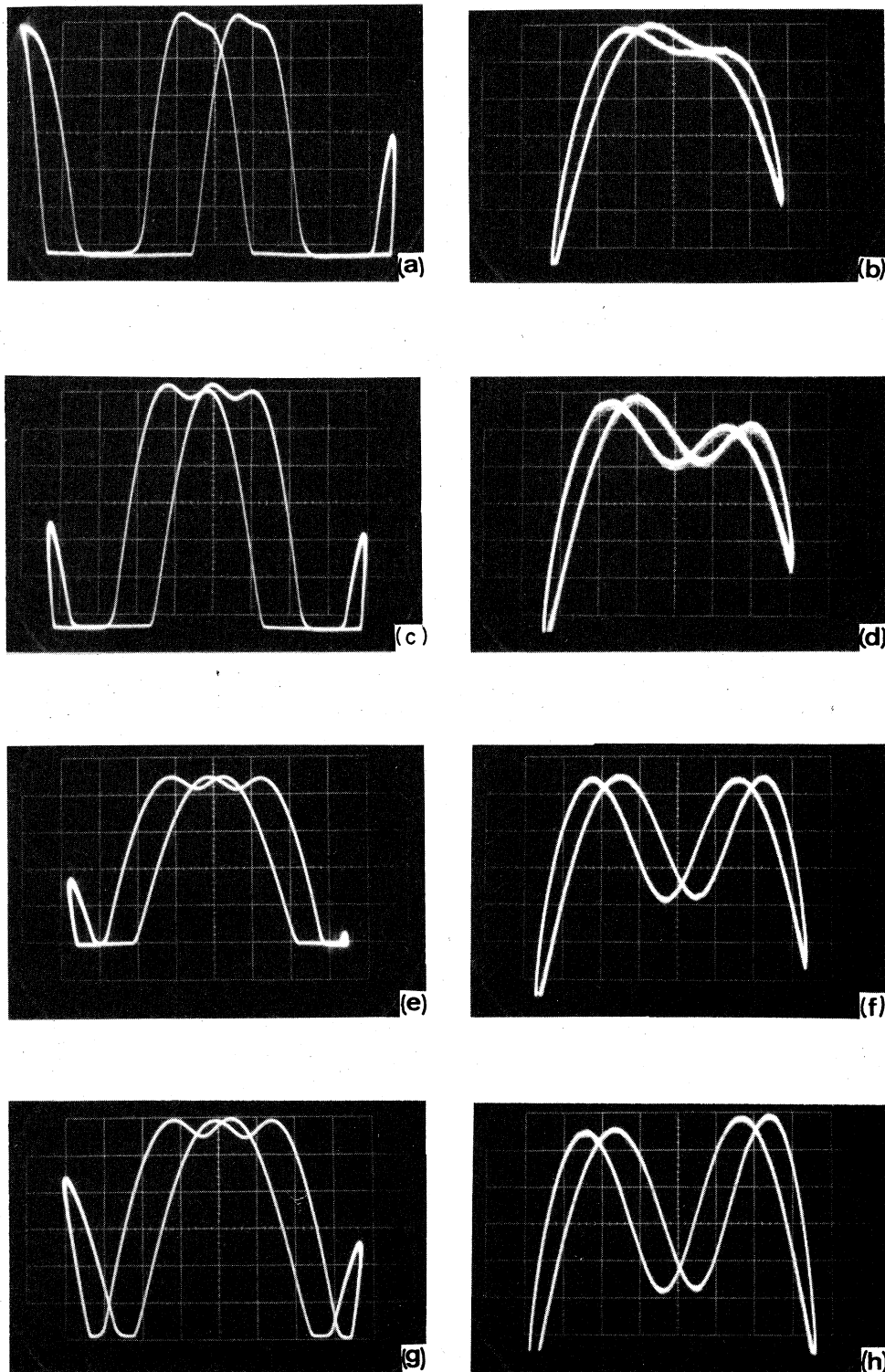


FIG. 8. Experimental line shapes obtained when the second tube is on the concave-mirror side (configuration 4 of Table I). Discharge currents are  $i_0 = 7$  mA in (a) and (b),  $i_c = 7.3$  mA in (c) and (d),  $i_c = 8.4$  mA in (e) and (f), and  $i_c = 8.9$  mA in (g) and (h). (b), (d), (f), and (h) are, respectively, magnifications of Lamb-dip regions of (a), (c), (e), and (g). Magnification factors are  $X \times 2.5$  everywhere,  $Y \times 2$  in (b),  $Y \times 4$  in (d), and  $Y \times 10$  in (f) and (g). From (a) to (c) sensitivity has been divided by two and from (a) to (e) and (g) by five. The prominent feature of these curves is the passage from the lf to the hf type of asymmetry with increasing current. In (a),  $f = 5.8 \times 10^{-2}$ , in (c),  $f = 3.4 \times 10^{-2}$ , in (e),  $f \approx 0$ , and in (g),  $f = -6 \times 10^{-3}$ . The interpretation follows from Table I. At weak intensities, population effects are stronger and force the asymmetry to be of the lf type [(a)–(d)]. However, when the gain is increased, the saturation effect also increases and changes the type of asymmetry.

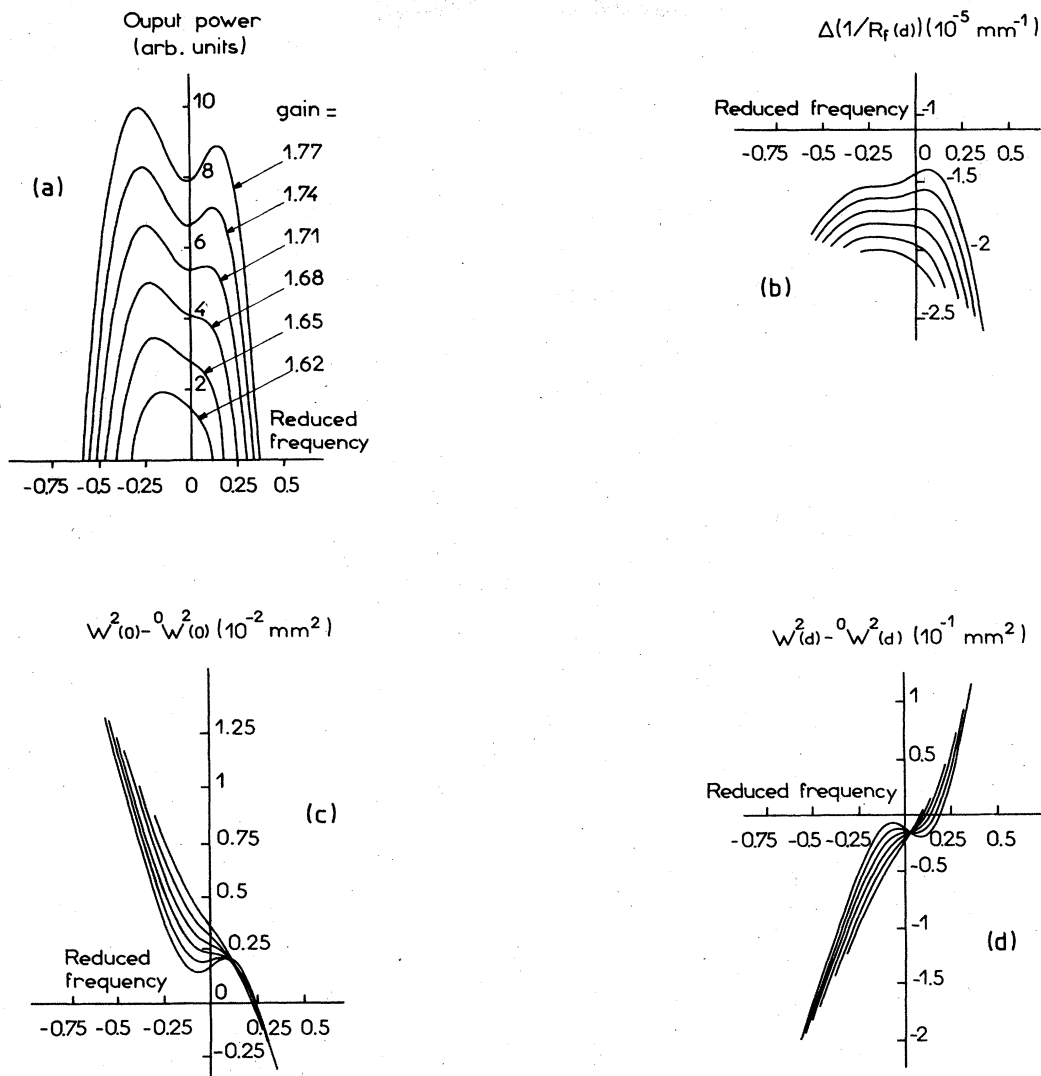


FIG. 9. Theoretical curves corresponding to configuration 4 of Table I, calculated with  $u = 2.26 \times 10^{-2}$  (corresponding to  $r_0 = 2.5$  mm). The high inhomogeneity of population influences line shape [in (a)] very much, giving a 1f type of asymmetry [compare with Fig. 5(a)]. It also lowers the curvature  $1/R_f(d)$  [in (b)], squeezing the curves as compared to those of Fig. 5(b). The same remark can be made for (c) and (d), where one sees the dispersion part of the curves due to saturation weakened in proportion to the part due to population [compare also with Figs. 5(c) and 5(d)].

then canceled by the asymmetry effect of the saturation inhomogeneity, in agreement with experiment (Fig. 8). The variations of spot sizes and beam curvatures are depicted in Figs. 10(b)–10(d). A comparison with Figs. 5(b)–5(d) and 9(b)–9(d) shows the influence of a variation in the inhomogeneity of population.

#### IV. CONCLUSION

In this paper we have given a series of results which show the influence of some macroscopic parameters on the line shape in a laser beam. They illustrate the complexity of the problem. The magnitude of the discharge current, the diameter of the amplifying tube, and the properties of the gas determine the inhomogeneity of pop-

ulation. The distribution of the electric field and thus the inhomogeneity of saturation are determined by the position of the amplifying tube, the length of the laser, the curvature of the mirrors, and the diameter of a diaphragm and its position. The asymmetry of a line results generally from a competition between the lens effects induced by the two types of inhomogeneities. It is that complexity which limits the usefulness of simple models in the explanation of line shapes. However, we have shown that, generally, the Gaussian beam model does permit the description of the variation of the diameter of a mode and, via Garside's effect, a qualitative prediction of line shapes. It should be noted that we have limited ourselves to the total output power. If one measures the intensity on the laser axis using a small area detector, it is possible

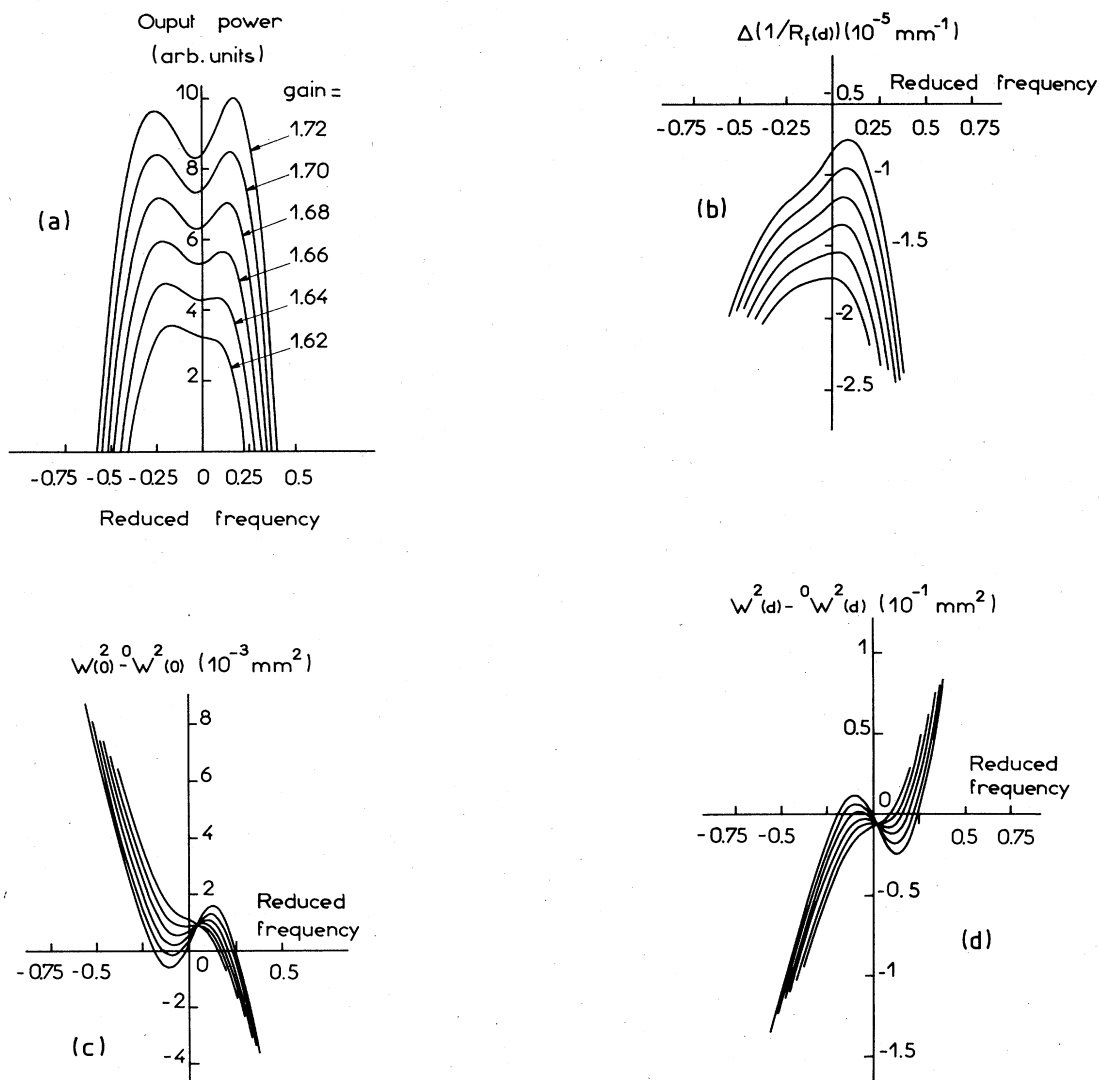


FIG. 10. Theoretical curves corresponding to configuration 4 of Table I, calculated with  $u = 1.57 \times 10^{-2}$  (corresponding to  $r_0 = 3$  mm). (a) shows in this case the same change of asymmetry as that observed in experimental results (Fig. 8): at low gains population effects predominate and for higher intensities saturation effects overpower them. All curves in this figure picture an intermediate case between the corresponding ones in Figs. 5 and 9. These figures illustrate the sensitivity of the laser line shape to the inhomogeneity of population when the tube is near the concave mirror, i.e., when the field and the population are characterized by a transverse variation length of the same order of magnitude. When comparing these results to those of Fig. 8, one should bear in mind that an increase of the intensity of the discharge current corresponds to a decrease of the inhomogeneity of population (the transverse distribution of amplifying atoms is flattened). Then results of Fig. 8 probably correspond to a lower value of  $u$  than those of Fig. 6 (or a higher value of  $r_0$ ), which justifies the use of  $r_0 = 3$  mm instead of the internal radius (2 mm) of the tube. Moreover, the variation of asymmetry of Fig. 8 also results from a decrease of  $u$  as  $i_c$  increases.

to find new phenomena due to the variation of the radius of curvature versus frequency. Such measurements are actually in progress in our laboratory.

The numerical methods we have recently developed give results which are in good agreement with measurements. In this work we have tried to explain in a qualitative manner how the different causes intervene in the formation of line shapes. In order to perform more quantitative studies one would have to use a more accurate expression for the polarizability, including, e.g., the influence of the field intensity on the lifetime of laser-active states.

With that effort one could perhaps show the influence of collisions on line shapes, study the microscopic properties of atoms in the laser, or introduce the geometric properties of the beam into the study of deterministic chaos, i.e., take a new step in the understanding of phenomena currently observed.

#### ACKNOWLEDGMENTS

We are happy to thank Mr. H. Gehanno, Mr. P. Guichard, Mr. A. Kellou, Mr. J. Roignant, and Mr. J. Sorieux who helped us in the course of this work.

- <sup>1</sup>W. E. Lamb, Jr., *Phys. Rev.* **134**, A1429 (1964).  
<sup>2</sup>A. Szöke and A. Javan, *Phys. Rev. Lett.* **10**, 521 (1963).  
<sup>3</sup>R. A. McFarlane, W. R. Bennett, Jr., and W. E. Lamb, Jr., *Appl. Phys. Lett.* **2**, 189 (1963).  
<sup>4</sup>A. Szöke and A. Javan, *Phys. Rev.* **145**, 137 (1966).  
<sup>5</sup>P. W. Smith, *J. Appl. Phys.* **37**, 2089 (1966).  
<sup>6</sup>R. H. Cordover and P. A. Bonczyk, *Phys. Rev.* **188**, 696 (1969).  
<sup>7</sup>B. L. Gyorffy, M. Borenstein, and W. E. Lamb, Jr., *Phys. Rev.* **169**, 340 (1968).  
<sup>8</sup>R. L. Fork and M. A. Pollack, *Phys. Rev.* **139**, A1408 (1965).  
<sup>9</sup>H. K. Holt, *Phys. Rev. A* **2**, 233 (1970).  
<sup>10</sup>A. D. White, *Appl. Phys. Lett.* **10**, 24 (1967).  
<sup>11</sup>Y. V. Troitskii and V. P. Chebotaev, *Opt. Spektrosk.* **20**, 362 (1966) [*Opt. Spectrosc. (USSR)* **20**, 199 (1966)].  
<sup>12</sup>I. P. Mazanko, M. I. Molchanov, N. D. D. Ogurok, and M. V. Sviridov, *Opt. Spektrosk.* **30**, 927 (1971) [*Opt. Spectrosc. (USSR)* **30**, 495 (1971)].  
<sup>13</sup>P. A. Wolff, N. B. Abraham, and S. R. Smith, *IEEE J. Quantum Electron.* **QE-13**, 400 (1977).  
<sup>14</sup>L. A. Schlie and J. T. Verdeyen, *IEEE J. Quantum Electron.* **QE-5**, 21 (1969).  
<sup>15</sup>W. R. Bennett, Jr., *Appl. Opt. Suppl.* **2**, 3 (1965).  
<sup>16</sup>A. G. Fox and T. Li, *IEEE J. Quantum Electron.* **QE-2**, 774 (1966).  
<sup>17</sup>H. W. Kogelnik, *Bell. Syst. Tech. J.* **44**, 455 (1965); *Appl. Opt.* **4**, 1562 (1965); H. W. Kogelnik and T. Li, *ibid.* **5**, 1550 (1966).  
<sup>18</sup>L. W. Casperson and A. Yariv, *Appl. Phys. Lett.* **12**, 355 (1968).  
<sup>19</sup>R. Y. Chiao, E. Garmire, and C. H. Townes, *Phys. Rev. Lett.* **13**, 479 (1964).  
<sup>20</sup>A. Javan and P. L. Kelly, *IEEE J. Quantum Electron.* **QE-2**, 470 (1966).  
<sup>21</sup>C. Freed and H. A. Haus, *IEEE J. Quantum Electron.* **QE-9**, 219 (1973).  
<sup>22</sup>H. Maeda and K. Shimoda, *J. Appl. Phys.* **46**, 1235 (1975).  
<sup>23</sup>B. K. Garside, *IEEE J. Quantum Electron.* **QE-4**, 940 (1968).  
<sup>24</sup>R. L. Barger and J. L. Hall, *Phys. Rev. Lett.* **22**, 4 (1969).  
<sup>25</sup>G. Kramer, C. O. Weiss and J. Helmcke, *Z. Naturforsch.* **30a**, 1128 (1975).  
<sup>26</sup>G. Stephan and H. Taleb, *J. Phys. (Paris)* **42**, 1623 (1981).  
<sup>27</sup>G. Stephan, H. Taleb, F. Legros, and C. Pesty, *J. Phys. (Paris)* **43**, 255 (1982).  
<sup>28</sup>A. Le Floch, R. Le Naour, J. M. Lenormand, and J. P. Taché, *Phys. Rev. Lett.* **45**, 544 (1980).  
<sup>29</sup>A. Le Floch, J. M. Lenormand, R. Le Naour, and J. P. Taché, *J. Phys. (Paris) Lett.* **43**, L493 (1982).  
<sup>30</sup>G. Stephan, *J. Phys. (Paris) Lett.* **44**, L361 (1983).  
<sup>31</sup>P. Cérez and R. Felder, *Appl. Opt.* **22**, 1251 (1983).  
<sup>32</sup>G. Stephan and M. Trümper, *Phys. Rev. A* **28**, 2344 (1983).  
<sup>33</sup>G. Stephan and M. Trümper, *Phys. Rev. A* **28**, 3450 (1983).  
<sup>34</sup>G. Stephan and M. Trümper, *J. Phys. (Paris) Lett.* (to be published).  
<sup>35</sup>S. Asami, H. Gamo, and T. Tako, *Jpn. J. Appl. Phys.* **22**, 88 (1983); **22**, 94 (1983).  
<sup>36</sup>C. J. Bordé, J. L. Hall, C. V. Kunasz, and O. G. Hummer, *Phys. Rev. A* **14**, 236 (1975); C. J. Bordé, G. Camy, and B. Decomps, *ibid.* **20**, 254 (1978).  
<sup>37</sup>G. Stephan, R. Le Naour, and A. Le Floch, *Phys. Rev. A* **17**, 733 (1978).

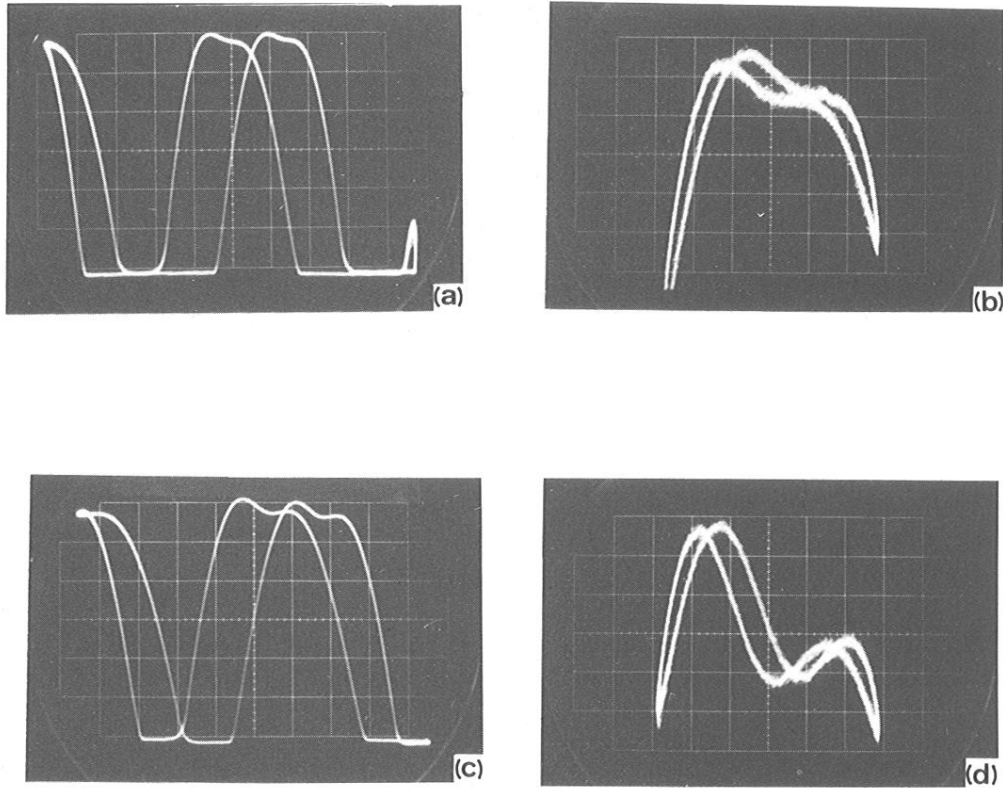


FIG. 2. Laser output vs frequency for configuration 1 of Table I (tube 1 on plane-mirror side). Intensities are in arbitrary units. Frequencies increase from left to right. For the cavity used,  $c/2d = 263$  MHz indicating that a division on the horizontal scale is 45 MHz [in (a) and (c)]. Doubling and deformation of the curves result from hysteresis and nonlinearity effects of the piezoelectric ceramic. (a) and (c) show entire line shapes while (b) and (d) are magnifications of Lamb-dip regions [ $X \times 2.5$  and  $Y_{(a)} \times 5$  for (b) and  $Y_{(c)} \times 10$  for (d)]. A diaphragm 3.5 mm in diameter is set on the concave mirror and this feature is the same for the other experimental results given in this paper. Results are shown for two values of the discharge current:  $i_c = 11$  mA [in (a) and (b)] and  $i_c = 13.5$  mA [in (c) and (d)] where intensity is two times greater. The asymmetry of the line is of lf type. It is due to saturation inhomogeneity and increases linearly with intensity. The factor of asymmetry as defined by Freed and Haus (Ref. 21) is  $f = 2(H - h)/(H + h)$ , where  $H$  and  $h$  are, respectively, the intensities at lf and hf maximum. In (a),  $f = 2.2\%$ , in (b),  $f = 4.2\%$ .



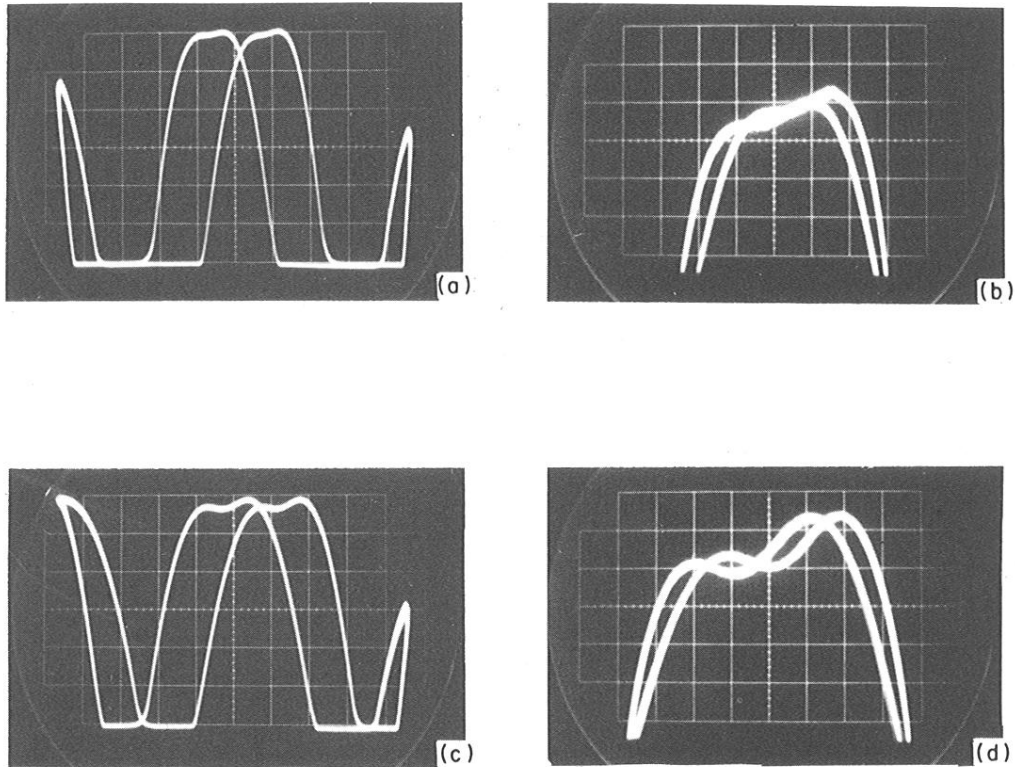


FIG. 4. Experimental line shapes obtained when tube 1 (large bore) is placed on the concave-mirror side (configuration 2 of Table I). Discharge currents are 11 mA [in (a) and (b)] and 13.5 mA [in (c) and (d)]. Intensities are about five times greater than those given in Fig. 2. Magnification factors are  $X \times 2.5$  and  $Y \times 5$  for (b) and (d). Intensity is two times greater in (c) than in (a). The lines show a hf type of asymmetry due to saturation. We find  $f = 1.6 \times 10^{-2}$  in (a) and  $f = 3.5 \times 10^{-2}$  in (c). In this configuration, pumping of energy is much more efficient than in the previous experiment because the volume of the mode is greater. This is why the saturation effect becomes greater than the population one.

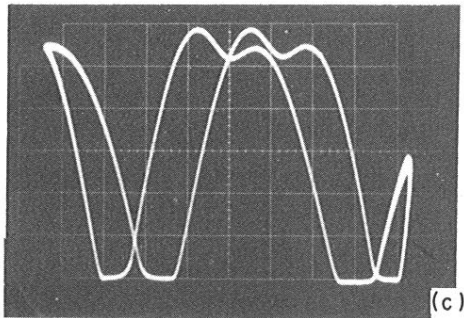
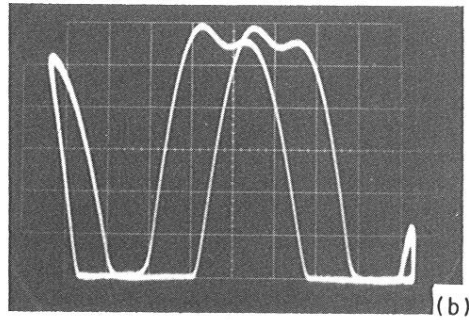
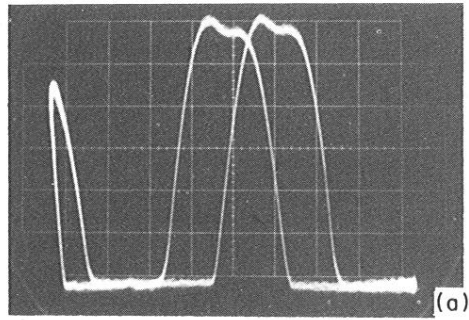


FIG. 6. Experimental line shapes obtained when the narrow amplifying tube is on the side of the plane mirror (configuration 3 of Table I). Discharge currents are  $i_c = 4.5$  mA (a),  $i_c = 5$  mA (b), and  $i_c = 6$  mA (c). While currents are lower, densities are stronger in this tube than in the other. Intensity in (c) is two times that of (b) which is also two times that of (a). Asymmetries are of the lf type as in configuration 1 (Fig. 2) but more pronounced due to a greater gain coming from the greater density of the discharge current. In (a),  $f = 3.2 \times 10^{-2}$ ; in (b),  $f = 5.2 \times 10^{-2}$ ; and in (c),  $f = 7.2 \times 10^{-2}$ , showing that the asymmetry does not increase linearly with intensity.

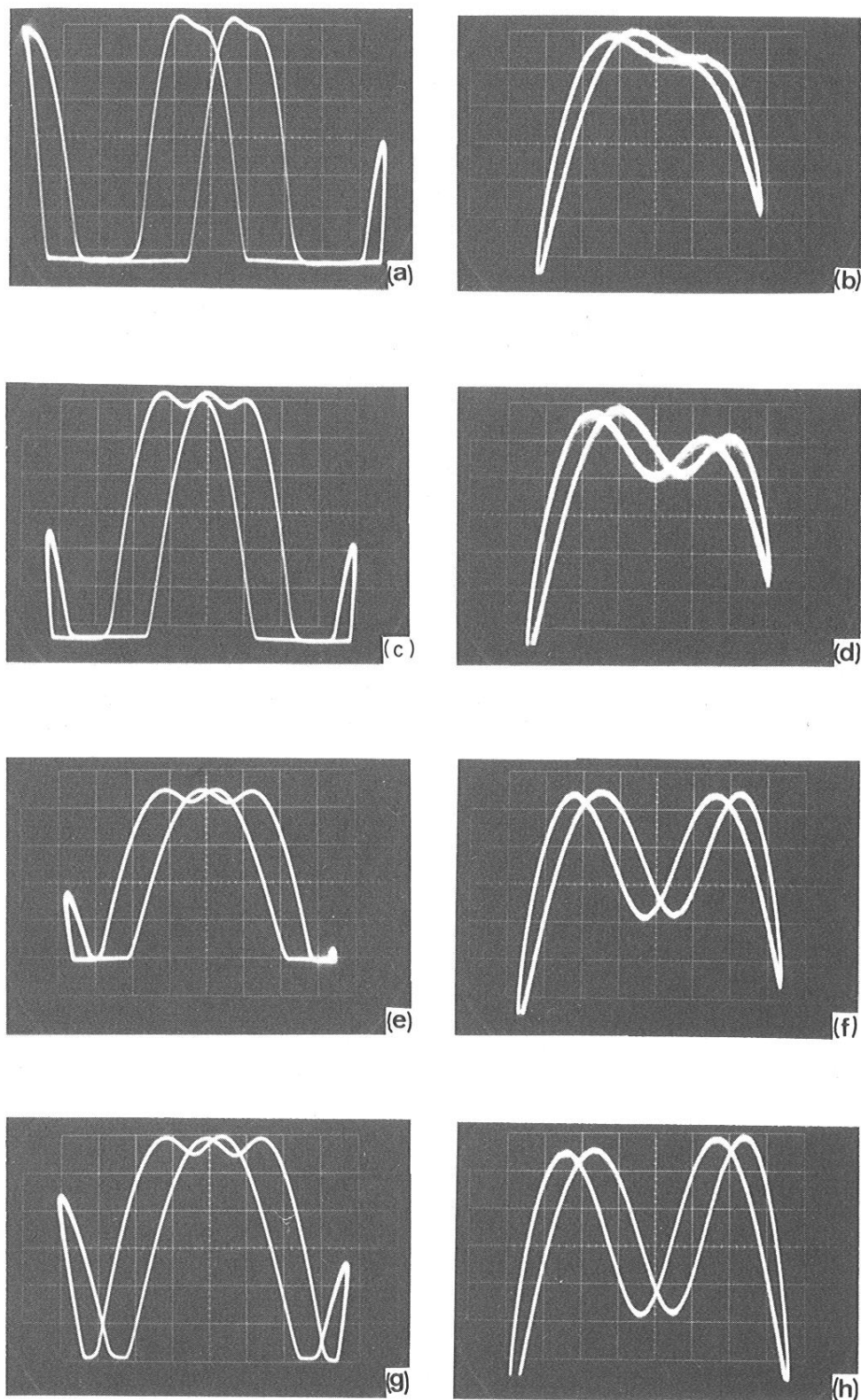


FIG. 8. Experimental line shapes obtained when the second tube is on the concave-mirror side (configuration 4 of Table I). Discharge currents are  $i_0 = 7$  mA in (a) and (b),  $i_c = 7.3$  mA in (c) and (d),  $i_c = 8.4$  mA in (e) and (f), and  $i_c = 8.9$  mA in (g) and (h). (b), (d), (f), and (h) are, respectively, magnifications of Lamb-dip regions of (a), (c), (e), and (g). Magnification factors are  $X \times 2.5$  everywhere,  $Y \times 2$  in (b),  $Y \times 4$  in (d), and  $Y \times 10$  in (f) and (g). From (a) to (c) sensitivity has been divided by two and from (a) to (e) and (g) by five. The prominent feature of these curves is the passage from the lf to the hf type of asymmetry with increasing current. In (a),  $f = 5.8 \times 10^{-2}$ , in (c),  $f = 3.4 \times 10^{-2}$ , in (e),  $f \approx 0$ , and in (g),  $f = -6 \times 10^{-3}$ . The interpretation follows from Table I. At weak intensities, population effects are stronger and force the asymmetry to be of the lf type [(a)–(d)]. However, when the gain is increased, the saturation effect also increases and changes the type of asymmetry.